Errors induced by ozone field horizontal inhomogeneities into simulated nadir-viewing orbital backscatter UV measurements

Martin Felder,[1,2] Paul Poli,[3] and Joanna Joiner[1]

Received 15 October 2005; revised 2 August 2006; accepted 25 August 2006; published 4 January 2007.

[1] Radiative transfer calculations for nadir-viewing satellites normally assume the atmosphere to be horizontally homogeneous. Yet it has been shown recently that horizontal gradients can lead to significant errors in satellite infrared and microwave soundings. We extend the methodology to nadir backscatter ultraviolet forward modeling and present a first estimate of the effect's magnitude. The Solar Backscatter Ultraviolet/2 (SBUV/2) instrument, a nadir sounder, serves as our test bed. We find that the RMS error in calculated SBUV radiance induced by ozone inhomogeneities ranges between 0.05 and 0.3% (0.1–0.5%) for the 318 nm (306 and 313 nm) channel. The lower (higher) estimate corresponds to soundings with small (high) solar zenith angle. Occurrence of higher errors, particularly at wavelengths longer than 300 nm, coincides with some of the most interesting atmospheric phenomena like tropopause folds and the south polar ozone hole. This leads to a seasonal variation of the magnitude of the effect. Because of the mostly zonal variability of the ozone distribution, there is also the possibility that biases may be introduced, which is particularly critical if the data are to be assimilated or used to determine trends. The results presented are tested for robustness using different model atmospheres.

Citation: Felder, M., P. Poli, and J. Joiner (2007), Errors induced by ozone field horizontal inhomogeneities into simulated nadir-viewing orbital backscatter UV measurements, *J. Geophys. Res.*, *112*, D01303, doi:10.1029/2005JD006769.

1. Introduction

[2] It has been known for a while that collocations of ground-based measurements with satellite pixels, which rarely sample the same air mass, suffer from errors due to the horizontal variability of the atmospheric quantity considered [e.g., *Lambert et al.*, 1998; *Fioletov et al.*, 1999]. This effect is also relevant for satellite retrievals, and assimilation of retrievals or radiances. Radiative transfer models (RTMs) of the atmosphere commonly assume that the radiances measured by Earth-observing satellites pass through a horizontally homogeneous atmosphere. Depending on the variability of the atmospheric parameters or trace gas species observed, this assumption may induce random and/or systematic errors into the calculations.

[3] For limb-sounders, this realization has led to the development of two-dimensional retrieval algorithms, which deal with entire atmospheric slices at a time. For instance, *Worden et al.* [2004] have found the information content of simulated Thermal Emission Spectrometer CO retrievals to be higher by an order of magnitude for two-dimensional versus one-dimensional retrievals. *Poli and Joiner* [2004] and *Poli* [2004] report that horizontal gradients are also important for Global Positioning System radio occultation soundings. Recently, investigations have begun regarding the effect of temperature inhomogeneities on scanning nadir infrared and microwave sounders [*Joiner and Poli*, 2005]. While generally negligible, the effect was found to be considerable in some situations.

[4] This paper examines the magnitude of ozone inhomogeneities observed by a nadir-viewing instrument merely due to variation of the solar zenith angle (SZA) and solar azimuth angle (SAA). Observation times and locations of the SBUV instrument and ozone analyzed fields are used to simulate the effects of horizontal inhomogeneities on radiance calculations. To this end, analysis fields and SBUV data are described in section 2, along with geometrical considerations. Section 3 focuses on the differences between ozone seen along the slant and nadir ray path. Section 4 transforms these differences into radiance space. Simulated radiance differences for SBUV are computed from three different model fields, and the sensitivity toward the model field is investigated. Section 5 discusses the relevance of the effect in practice, and highlights some considerations for the future.

2. Data and Methods

2.1. Ozone Analyzed Fields

[5] The global ozone field from an SBUV radiance assimilation system [*Müller et al.*, 2004] based on earlier

[1]Laboratory for Atmospheres, NASA Goddard Space Flight Center, Greenbelt, Maryland, USA.
[2]Now at Leibniz Computing Centre, Garching, Germany.
[3]Centre National de Recherches Météorologiques, Météo-France, Toulouse, France.

Copyright 2007 by the American Geophysical Union.
0148-0227/07/2005JD006769

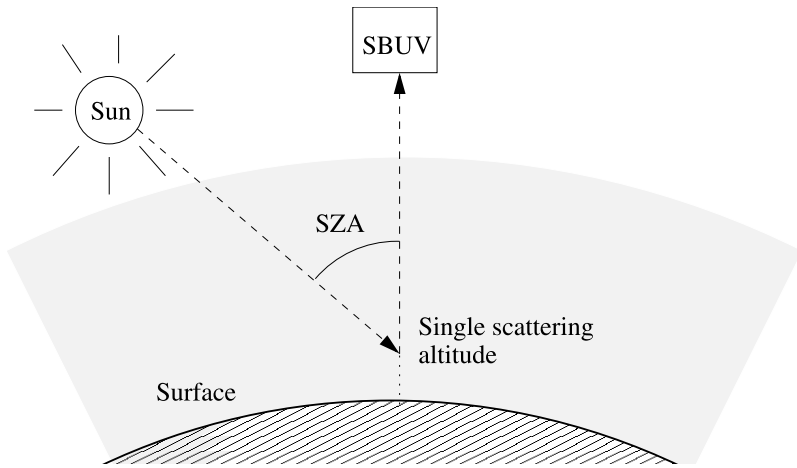

Figure 1. Sketch of the observation geometry.

work by *Stajner et al.* [2001] and *Riishøjgaard et al.* [2000] is used for representing ozone gradients in the atmosphere. The ozone analyzed fields generally compare to ozone sondes and limb-sounders with an RMS difference of 5–10% above 50 hPa, which rises to 40% at the tropopause (200 hPa), and stays mostly constant below it. The observation-minus-forecast RMS for a 6-hour assimilation of SBUV is about 10 DU. The Chemistry and Transport Model (CTM) used for the assimilation is driven by an online version of the GEOS-4 meteorological assimilation [*Lin*, 2004, and references therein]. This system features a horizontal resolution of 1.25° longitude × 1.0° latitude and generates analyses on 36 pressure levels between 1000 and 0.2 hPa. Since we expect to find significant inhomogeneity effects where strong ozone gradients are present, the periods of 2–4 March 2003 (strong northern hemisphere (NH) ozone gradients) and 16–17 October 2003 (strong south polar ozone gradients) were selected for the various case studies presented.

2.2. SBUV Data and Geometry

[6] The SBUV/2 instrument used here is a 12-channel nadir scanner with a 200 km × 200 km footprint, circling the Earth on a Sun-synchronous orbit on board the National Oceanic and Atmospheric Administration's satellite 16 (NOAA 16), with an equator crossing at 1430 local time (for the ascending orbit). We use SBUV as a shorthand for SBUV/2 throughout this paper. Depending on atmospheric absorption and scattering properties at the wavelength in question (here between 256 and 331 nm, see Table 1), not all ozone in a given column will be perceived by the satellite instrument. Figure 1 shows the solar backscatter observation geometry. In order to get an approximate light path for the atmospheric backscattered radiance I, SZA and SAA are calculated for each SBUV observation location and time at the surface. Variation of the SZA with altitude is neglected, and the SAA does not vary with height.

[7] The SBUV instrument has its highest sensitivity above the ozone peak, between 5 and 50 hPa [*Bhartia et al.*, 1996]. Here, retrieved ozone profiles agree to sondes and limb-sounders with about 6% RMSE. Below the ozone peak, there is essentially only one piece of ozone information in the SBUV spectra. The total ozone column is obtained by integrating the retrieved profile, and believed to be 2–3% accurate [*Labow et al.*, 2004].

[8] The Sun-normalized radiances measured by the SBUV instrument are usually given in "N-values," whereby

$$\boldsymbol{N} = -100 \log_{10} (\boldsymbol{I}/\boldsymbol{I}_0). \tag{1}$$

A radiance difference of $\Delta N = 1$ thus translates into a 2.33% relative difference between the corresponding intensities I. The effect of the slanted incidence can be estimated using the linear approximation

$$\Delta \boldsymbol{N} = \boldsymbol{J}(\boldsymbol{x}_{\text{slant}} - \boldsymbol{x}_{\text{nadir}}), \tag{2}$$

where x_{slant} and x_{nadir} are the interpolated analysis fields for slant and nadir path, integrated to yield 21 partial ozone columns on half umkehr layers, as given in the SBUV retrievals. We can define the Jacobian $\boldsymbol{J}$ of the SBUV RTM for channel i and layer j as

$$(\boldsymbol{J})_{ij} = \frac{\partial N_i}{\partial x_j}. \tag{3}$$

[9] We use this Jacobian to project ozone fields onto UV radiances. The same approximation is used for the SBUV

Table 1. SBUV/2 Channels and Wavelengths λ Used Throughout This Paper[a]

Channel	λ Actual, nm	λ Nominal, nm	λ Rounded, nm
1	252.00	252.2	252
2	273.61	273.5	274
3	283.10	283.0	283
4	287.70	287.6	288
5	292.29	292.2	292
6	297.59	297.6	298
7	301.97	301.9	302
8	305.87	305.8	306
9	312.57	312.5	313
10	317.56	317.6	318
11	331.26	331.2	331

[a]To avoid confusion, all references are made to the rounded wavelengths.

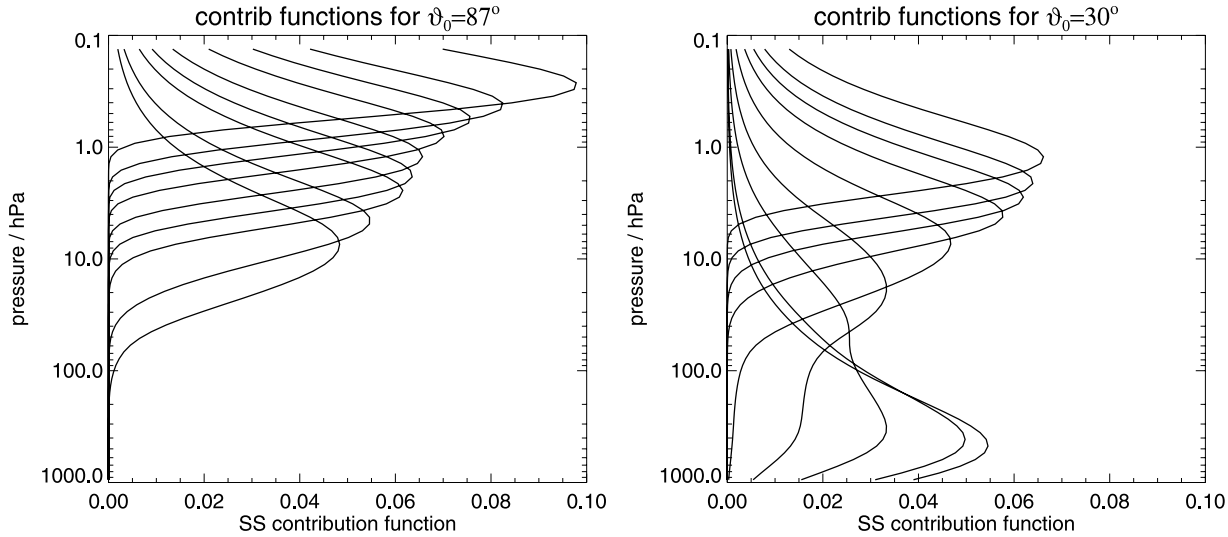

Figure 2. Single scattering (SS) contribution functions for SBUV channels at different SZA for a typical ozone profile (267 DU). The normalized contribution function ($\delta I_{SS}/\delta \ln p)(1/I)$ is displayed, with I_{SS} denoting the SS component of the measured radiance I. The channel wavelengths in nm, from top to bottom, are 274, 283, 288, 292, 298, 302, 306, 313 and 318. (Plot adapted from *Bhartia et al.* [1996, Figure 2].)

radiance assimilation [*Müller et al.*, 2004]. In order to check the RTM linearization for our purposes, one day in early March and one day under ozone hole conditions were scrutinized using a full RTM, namely TOMRAD, which includes all orders of scattering. For the cases detailed in section 3 with relative differences larger than 0.44% (i.e., $\Delta N = 0.2$), the approximation was found to produce mean errors of <0.002% up to channel 7, in the order of 0.01% for channels 8 and 9, and 0.08% for channel 10, which is the last channel used for retrievals. Hereby the linearized scheme is quite conservative in that it systematically underestimates the accurately calculated differences at long wavelengths by about 10%, independent of the SZA. Bearing these facts in mind, the linearized scheme is used throughout the remainder of the paper.

2.3. Approximation of the Ray Path

[10] To get an estimate for the average photon path through the atmosphere, the effective single scattering altitude for the incoming solar radiation first has to be estimated. Different arguments can be made in this regard, but we chose the peak of the single scattering contribution function (CF) for each SBUV channel as shown in Figure 2. A derivation of these functions is given by *Bhartia et al.* [1996]. The function shapes vary strongly with wavelength, solar zenith angle and ozone profile, less so with the atmospheric temperature profile, which is provided with the SBUV retrievals and originates from a sonde-derived climatology. Note that for the purpose of calculating the contribution functions, the nadir ozone profile at each pixel location is obtained by linearly interpolating the analysis, i.e., horizontal homogeneity is assumed. The resulting scattering altitudes for all 11 channels considered are depicted in Figure 3. For extreme SZAs, UV radiation does not penetrate into the lower atmosphere, but the altitude variability is also higher because of the wider range of possible ozone values in the extratropics [e.g., *Hudson et al.*, 2003].

[11] With the direction and penetration depth known, the effective geometric ray path can be calculated using the same method as used by *Poli and Joiner* [2004]. In this manner, latitude and longitude are obtained for each location where the ray path penetrates one of the 36 analysis

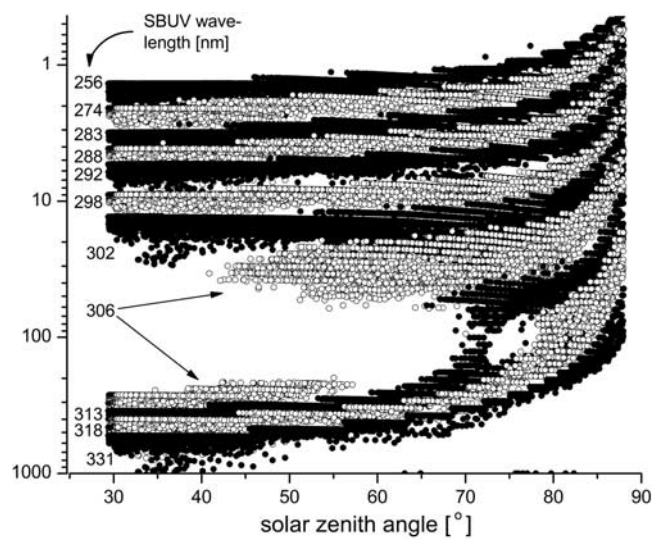

Figure 3. Scattering altitude for all SBUV channels, defined as the maximum of the single scattering CFs. The date range is 3–7 September 2003. The gap in the altitude range between 12 and 20 km (~50–200 hPa) relates to the switch from stratospheric to tropospheric CF maximum. In a real atmosphere, the transition is more gradual through a nearly bimodal CF shape, as seen in Figure 2 (right) for the 302 and 306 nm channels.

levels. The ozone slant profile "seen" by the ray is then calculated by linearly interpolating the model field of each level to these locations. The finite range of scattering altitudes for each wavelength is not taken into account. Figure 4 shows the variation of penetration depth and direction for those SBUV pixels which exhibit a noticeable difference between the paths. This gives an impression of the horizontal separation between the scattering location at nadir, and the point where the ray enters the model atmosphere (about 60 km altitude).

3. Results for Ozone Profile Gradients

[12] In the following, we will compare the differences between the ozone profile seen by the incoming (= slant) and outgoing (= nadir) UV radiation. Obviously, measurements of top-of-atmosphere (TOA) backscattered radiation contain contributions from both path directions. Calculating exactly the contribution from each direction is beyond the scope of this study; We will therefore first treat the two paths separately, and then suggest an approximate scheme for combining them in the next section.

[13] As can be seen in Figure 4b, pixels of interest for channel 9 cluster around strong gradients in the total ozone field, because this channel penetrates the atmosphere already quite well. Figure 4a is somewhat harder to interpret: Comparing with Figure 2 we note that at high SZA the behavior of channel 8 is similar to channel 9, while at mid to low latitudes it shows larger differences, probably because its secondary CF maximum forms around the region of the subtropical tropopause break. However, note also that many of the plotted interesting pixels lie in high-latitude regions because their ray paths have a strong meridional component due to the satellite orbit geometry. At 70°S latitude where the ozone hole boundary is located, the model resolution is about 110 km × 50 km (latitude × longitude). Here, gradients along a 200 km longitudinal offset can hence be well resolved. Elsewhere, the ozone gradients have to be much stronger in order to be detectable. Two typical cases of large differences between profiles seen along the nadir and slant paths are depicted in Figure 5. These occurred at the fringe of the southern hemisphere (SH) ozone hole and at the boundary of an ozone poor region in the NH, which according to *Hudson et al.* [2003] would probably be classified as upper tropospheric Polar Front. In general, correlating the occurrence of high profile differences with the boundaries of Hudson's regimes would be an interesting experiment, but is beyond the scope of this paper.

[14] We note that for the cases considered, the ozone field varies noticeably along the horizontal: Differences of up to 10% are seen in the ozone mixing ratios of slant and nadir paths. This is consistent with the magnitude of slant path related collocation errors reported for zenith-viewing ground instruments as compared to satellites [*Lambert et al.*, 1998]. Integrating ozone along the slant and nadir ray path yields differences of up to 2 DU for channel 8 and 4.5 DU for channel 9. For the largest 5% of radiance differences (compare section 4), the correlation coefficient to total ozone differences is ~0.95. The slopes for the two channels are 1.6 DU/N-value and 3.1 DU/N-value, respectively. For shorter wavelengths, total ozone differences are marginal and weakly correlated to radiances.

[15] To assess the critical height regions for the profile differences globally, their variability was calculated for all 2370 SBUV retrieval locations of 16–17 October 2003 (Figure 6). The sunlight penetration depth depends on both SZA and wavelength, and in turn the differences between observed slant and nadir O_3 profiles depend on penetration depth, SZA and ozone variability above the scattering altitude. Therefore two maxima can be identified in Figure 6: At high SZA, the slant path is longest but the penetration depth is shallow. This leads to a maximum of slant-nadir variability at high altitudes, despite the fact that the ozone distribution is usually quite smooth in the midstratosphere and above. A second maximum develops at relatively low SZAs and altitudes for wavelengths reaching the troposphere, mostly in the region around the subtropical tropopause break, where O_3 variability is highest. As already noted by *Joiner and Poli* [2005], the horizontal offsets in the mid to lower troposphere are too small to cause appreciable ozone differences.

[16] It is also interesting to consider that because of consistent O_3 variation with latitude and systematic patterns in the viewing direction (compare Figure 4), there are also systematic biases between slant and nadir profiles (Figure 7), even in a global average. Regionally, it is clear that situations like the ones depicted in Figure 5 lead to larger biases. For instance, along the rim of the Antarctic ozone hole, the Sun is always seen toward the equator, and therefore toward higher ozone values, which in turn introduce a high bias in the nadir versus slant radiances at altitudes where ozone has been depleted inside the polar vortex. For applications that average the ozone field over time in some manner, like assimilation or the creation of climatologies, the tendency to look toward the equator may induce biases despite the many nonzonal features in the ozone field: To illustrate this in a simple experiment, the ozone gradients in zonal and meridional direction were calculated for daily TOMS gridded total ozone fields in January 2000. The global sum of gradient absolute values turn out to be equal for both directions to within 10% on a given day. However, if the experiment is repeated by averaging the TOMS data over 3, 5, 10 and 30 days prior to gradient calculation, the ratio of zonal to meridional gradient sum continually rises to 1.6 at 30 days. This demonstrates the largely zonal nature of the bulk of ozone variability, when observed over a longer time span.

[17] In order to estimate the robustness of the statistics displayed in Figures 6 and 7, the experiment was repeated with the currently operational SBUV v6 profile assimilation system [*Riishøjgaard et al.*, 2000; *Stajner et al.*, 2004] and the underlying CTM without any assimilation (Figure 7b). All runs were initialized with the same initial conditions, using an ozone field from a combined SBUV and limb sounder assimilation [*Wargan et al.*, 2005] for 31 December 2002. By March 2003 the model fields have diverged because of, among other factors, excessive Brewer-Dobson circulation in the CTM and a lower-stratospheric high bias from SBUV data in the SBUV v6 assimilation. The differences between the ozone fields are much smaller than the differences between SZA categories or wavelengths. It can hence be concluded that the results described in this paper

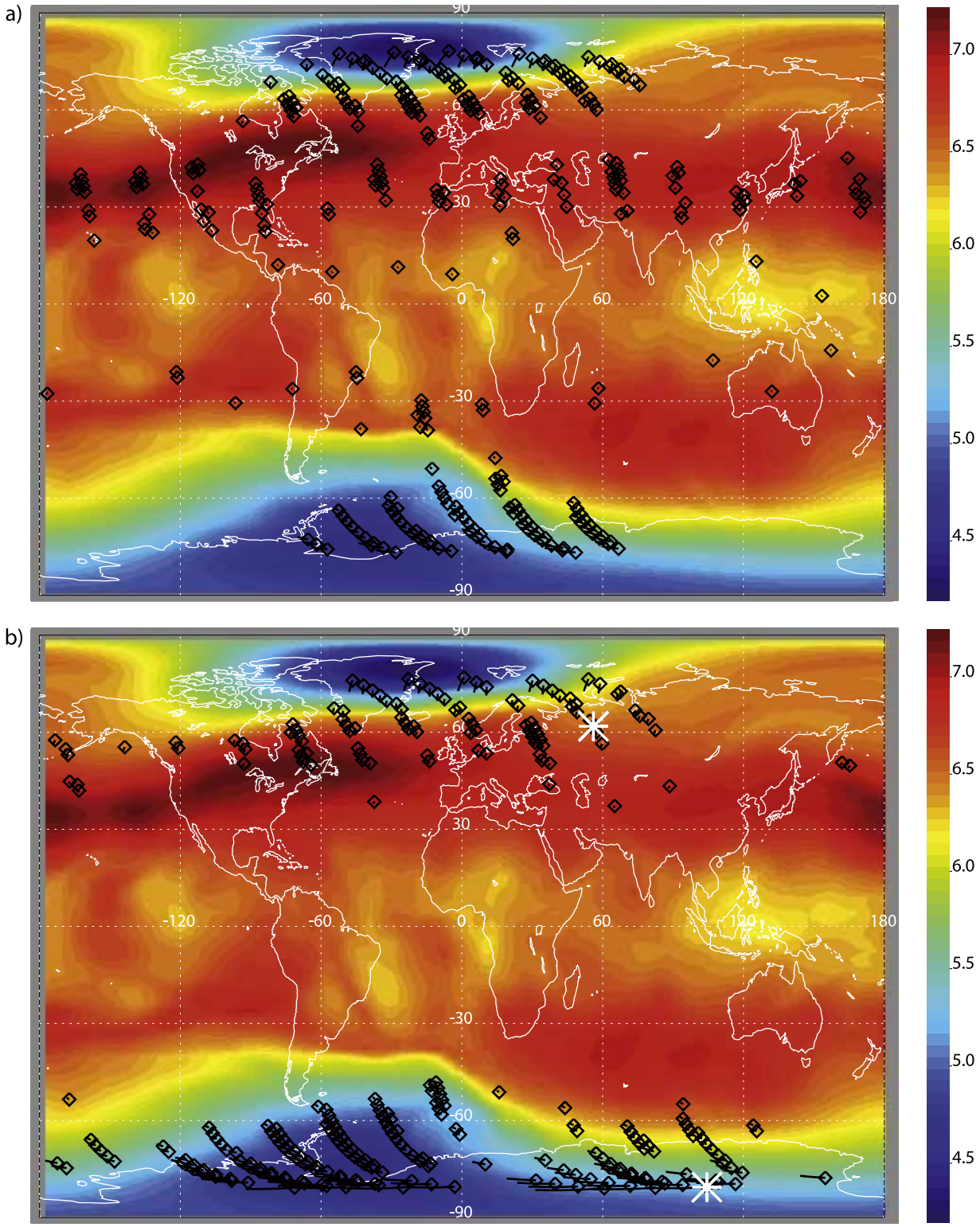

Figure 4. Surface projection of incoming ray path through the model atmosphere, i.e., from 0.2 hPa to scattering altitude. (a) SBUV channel 8 (306 nm) superimposed on the ozone volume mixing ratio at 5 hPa (in ppmv) of 17 October 2003, 0000 UTC and (b) same but using channel 9 (313 nm) and the total ozone field, in DU. Diamonds denote SBUV nadir points, measured within 24 hours around said time. Only the 5% of pixels with the largest radiance differences between simulated slant and nadir paths are shown. The two asterisks are the situations detailed in Figure 5.

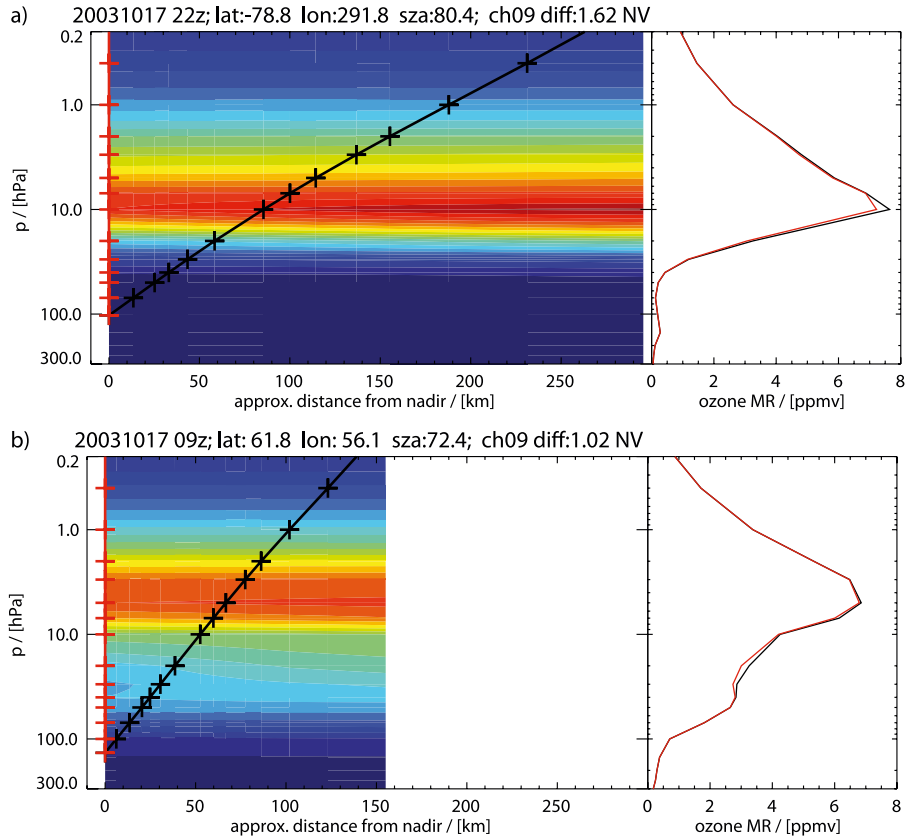

Figure 5. Incoming (black) and outgoing (red) raypath through the model atmosphere for two different situations for SBUV channel 9 (313 nm). The crosses denote model layers. Corresponding total ozone differences were (a) 4.06 DU and (b) 4.03 DU.

are also valid for other CTMs and assimilation procedures with similar spatial resolution.

4. Effect on SBUV Simulated Radiances

[18] To get an idea of the magnitude of the effect as seen by an orbital UV detector, Figure 8 shows the radiance difference for all SBUV pixels in the March case. For comparison, the measurement noise of the SBUV instruments has been estimated to be generally below 0.5% [*DeLand et al.*, 2004]. The largest differences for this time period occur at the location of the subtropical jet streams, as the light travels through the tropopause break and its strong ozone gradients. Again, the structures seen are very similar for the three ozone fields introduced in Figure 7b. Interestingly, while the free-running CTM does yield the smallest slant/nadir differences at almost all latitudes, it seems to produce more scatter around the jet streams. This may be explained by the fact that strong ozone gradients introduced by transport tend to get smoothed out by assimilating the vertically low resolved SBUV observations with imperfect forecast and observation covariance modeling [*Stajner et al.*, 2004].

[19] The distributions for the radiance differences feature a very strong central peak around zero, with thin tails that spread beyond the measurement noise (Figure 9). This is consistent with what *Joiner and Poli* [2005] found for the AIRS instrument. For the channels between 306 and 318 nm as many as 10–20% of the slant-nadir differences are larger than 0.5%. The selected ozone hole situation represents a rather extreme case, as can be seen from the seasonal variability of radiance differences shown in Figure 10.

[20] So far, we assessed the differences between radiances N_{nadir} and radiances N_{slant} calculated from forecast and analysis ozone fields for various SBUV channels. We now evaluate the impact these differences have on calculated SBUV radiances, which are needed in retrieval or assimilation schemes.

[21] It can be easily shown that with θ denoting the SZA,

$$N_{\mathrm{meas}} \simeq \frac{N_{\mathrm{nadir}} + N_{\mathrm{slant}} \sec\theta}{1 + \sec\theta} \tag{4}$$

is the first-order approximation in $\sec\theta$ for the measured SBUV radiance.

[22] In order to estimate the impact of a difference N_{slant} minus N_{nadir} into a calculated SBUV radiance, we consider equation (4) from a forward modeling point of view and note N_{calc} the SBUV radiance calculated from the ozone fields. For the particular case when we neglect the horizontal gradients (i.e., assuming $N_{\mathrm{nadir}} = N_{\mathrm{slant}}$):

$$N_{\mathrm{calc}}^{\mathrm{nogradient}} = N_{\mathrm{nadir}} \tag{5}$$

While for the other cases, we have

$$N_{\mathrm{calc}}(\theta) - N_{\mathrm{calc}}^{\mathrm{nogradient}} = \frac{N_{\mathrm{slant}} - N_{\mathrm{nadir}}}{1 + \cos\theta} \tag{6}$$

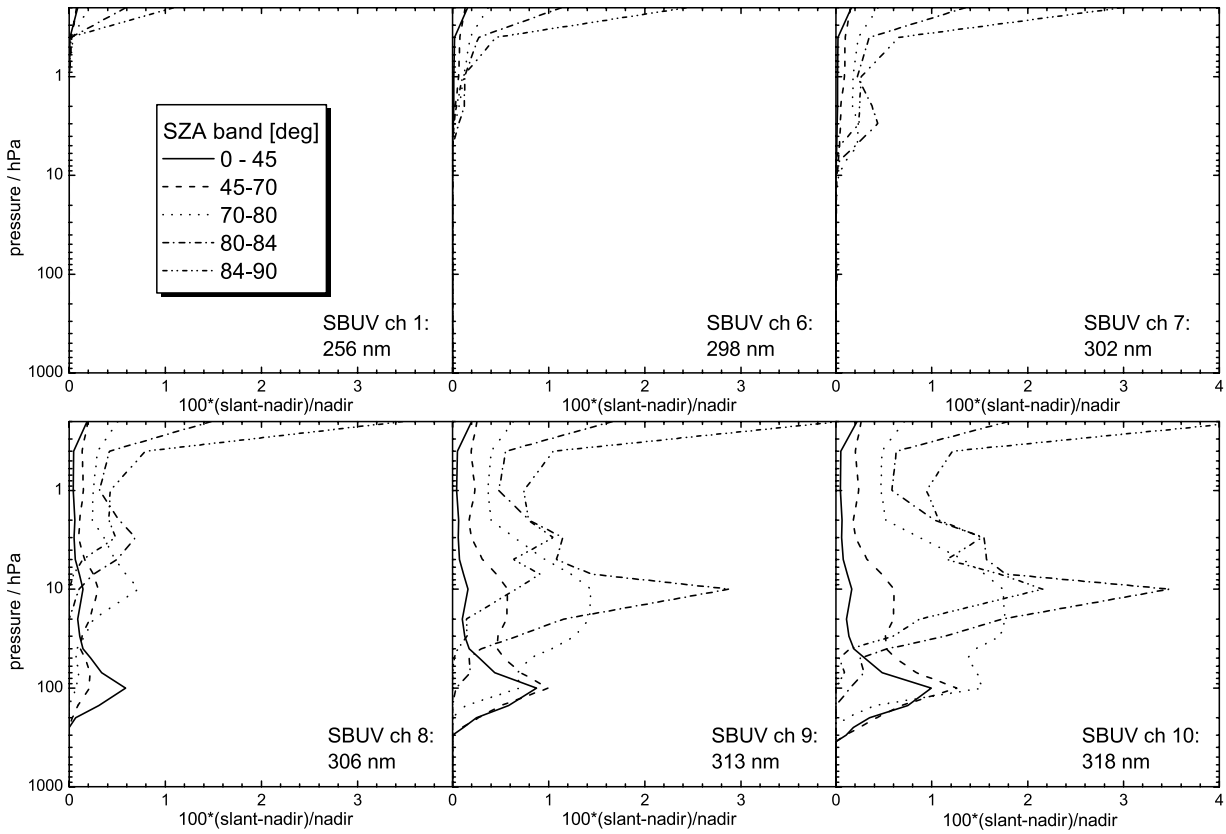

Figure 6. Standard deviation of differences between the ozone profile seen by the incoming (slant) and outgoing (nadir) radiation for SBUV channels 1 and 6 to 10.

Dividing both sides by equation (5):

$$\frac{N_{\mathrm{calc}}(\theta) - N_{\mathrm{calc}}^{\mathrm{nogradient}}}{N_{\mathrm{calc}}^{\mathrm{nogradient}}} = \frac{N_{\mathrm{slant}} - N_{\mathrm{nadir}}}{N_{\mathrm{nadir}}} \cdot \zeta(\theta) \tag{7}$$

where $\zeta(\theta)$ is a mapping function which projects the differences N_{slant} minus N_{nadir} into differences in SBUV radiance space:

$$\zeta(\theta) = \frac{1}{1 + \cos\theta} \tag{8}$$

Figure 11 shows that for small SZA, the effects of horizontal gradients are halved when projected in SBUV radiances. However, for highly slanted geometries (θ approaching 90°), ζ gets closer to one. This indicates that the differences N_{slant} minus N_{nadir} shown in this paper at high latitudes map directly and with only a small reduction into errors in the forward modeling of SBUV radiances.

[23] The results shown in Figures 9 and 10 should be read in light of Figure 11 to interpret the effect of ozone gradients on SBUV radiances. It thus appears that the RMS error induced by neglecting horizontal gradients in the ozone field when calculating SBUV radiances is most important for the three lowest peaking channels and varies between 0.05 and 0.5%. Among these three channels, the largest RMS errors in SBUV radiance are incurred for higher SZA and for the 306 and 313 nm channels. We note that these values could be used as inputs in data assimilation or data retrieval to formulate the contribution of horizontal inhomogeneities to the forward model variance error.

5. Conclusions and Future Directions

[24] The errors induced by ozone field horizontal gradients into simulated SBUV measurements are found to be only important for the 306, 313 and 318 nm channels. The RMS of these errors ranges from less than 0.05% for the 318 nm channel to 0.5% for soundings with high SZA (i.e., high latitude) for the other two channels. While only the latter estimate approaches the SBUV instrument noise, our study also indicates that such errors are reached for the most interesting structures in the ozone field, e.g., ozone (mini-) holes, the subtropical jet streams, the polar front and local phenomena like tropopause folds. Especially for field campaigns at high latitudes, which involve comparisons with satellite instruments, and for satellite validation in general [e.g., *Fioletov et al.*, 1999; *Lambert et al.*, 1998; *Labow et al.*, 2004] it would be advisable to take slant path offsets into account. Ideally, all ground-based and satellite instruments involved would use the same high-resolution analysis field as a basis for their retrievals. Most modern Earth-viewing satellites are cross-track or along-track scanners, where usually both incoming and outgoing path are slanted [cf. *Joiner and Poli*, 2005]. In particular, modern nadir-viewing ozone sounders like the Ozone Monitoring Instrument (OMI) on EOS Aura [*Levelt et al.*, 2006], and the Scanning Imaging Absorption Spectrometer for Atmospheric Chartography (SCIAMACHY) on ENVISAT [*Bovensmann*

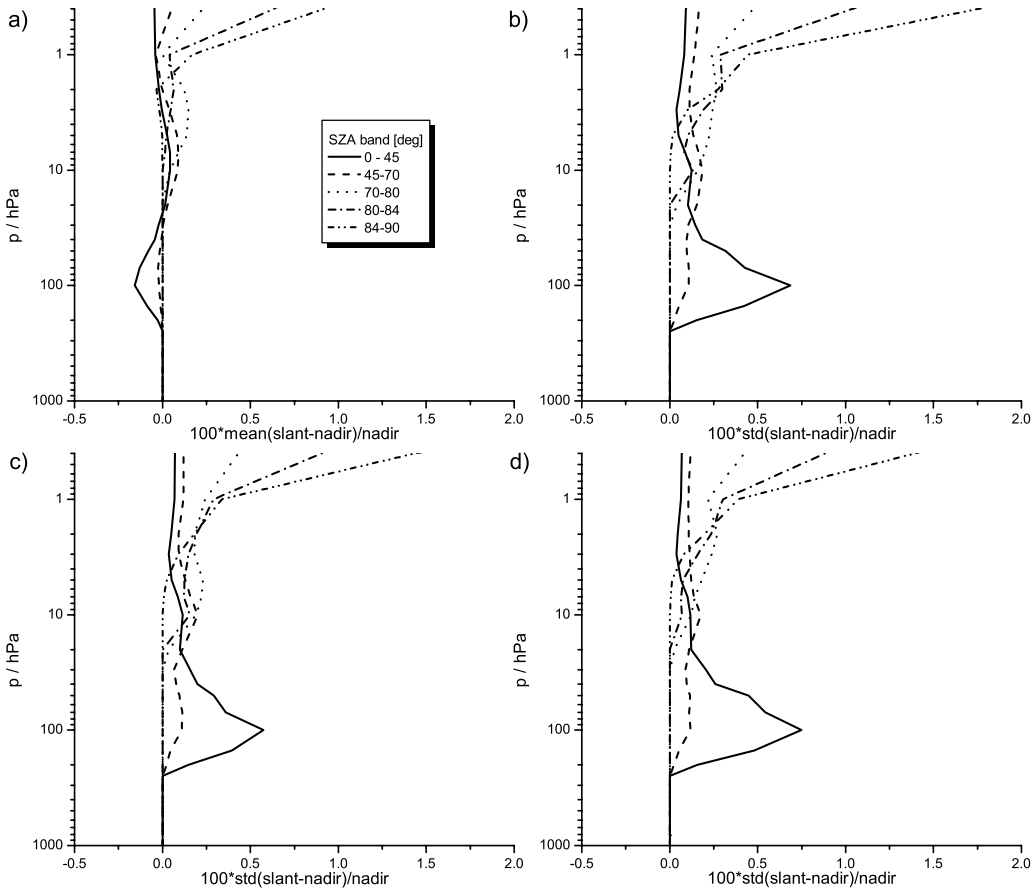

Figure 7. Same as Figure 6 but channel 8 (306 nm) only: (a) mean difference. Similar plots for the period 2–4 March 2003, where three different atmospheric model fields were available: standard deviation (std) for (b) radiance assimilation, as in Figure 6; (c) profile assimilation; and (d) no assimilation, CTM only.

et al., 1999] feature wide swaths that may, depending on the geometry, compensate for or exacerbate the inhomogeneity effect.

[25] Future developments in the field are expected to lead to satellite instruments with reduced noise and CTMs with increased accuracy and horizontal resolution. Both factors will render the effects described in this work more important to consider. The same applies to possible future atmospheric chemistry instruments in geostationary orbit or at the Lagrange points. As already mentioned in the introduction, limb-sounding ozone instruments like the one planned for the Ozone Mapping and Profiler Suite (OMPS) [*Dittman et al.*, 2002] are bound to profit most from taking into account horizontal ozone variations.

[26] *Joiner and Poli* [2005] reported that accounting for horizontal variability produced smaller differences between forecast and observed quantities in a meteorological assimilation system for infrared O_3 channels. After having quantified the SBUV forward modeling RMS error due to horizontal ozone inhomogeneities, a next step could be to conduct an error analysis in order the estimate the impact of these errors on ozone retrievals. Directions for further research also include modifying the radiance assimilation system to take into account horizontal variations. This involves adapting the slant algorithm to the internal assimilation background field on 55 layers, up to 0.01 hPa, and

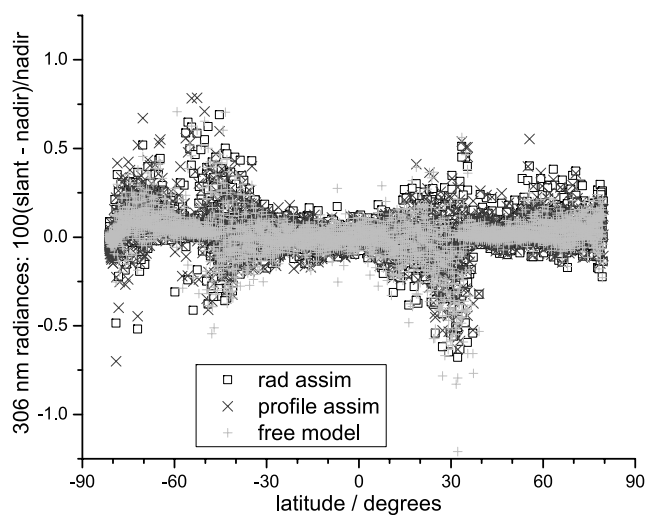

	mean [%]	σ [%]
Radiance assim.	$1.08 \cdot 10^{-2}$	$4.90 \cdot 10^{-2}$
Profile assim.	$8.77 \cdot 10^{-3}$	$4.72 \cdot 10^{-2}$
Free-running model	$3.36 \cdot 10^{-3}$	$5.22 \cdot 10^{-2}$

Figure 8. Differences in radiances calculated for SBUV channel 8 (~306 nm) from slant and nadir profiles of the three different model fields described in the main text, for 2–4 March 2003. The table lists the respective mean difference and standard deviation.

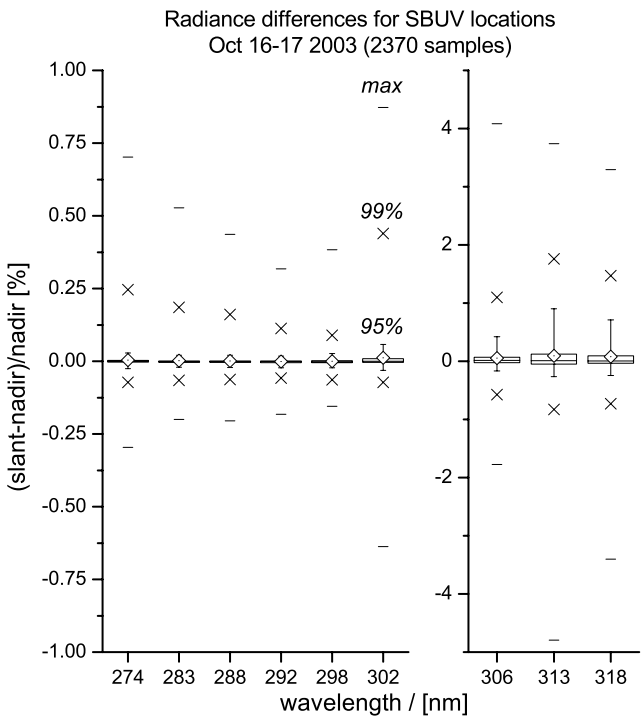

Figure 9. Box-and-whisker plots for the radiance differences of SBUV channels 2–10, on 16–17 October 2003. Boxes show the 75th percentiles and the median, and the diamond marks the mean. Whiskers mark the 95th percentile, crosses mark the 99th percentile, and dashes mark the absolute minimum/maximum values observed.

investigating the impact on the assimilation. The analyzed ozone fields used so far are not ideal for calculating corrections, because the assimilation step has been performed already, and the analysis downsampled to 36 levels. Still, for the limited sample of days investigated, a preliminary calculation (not shown) of simulated radiances for SBUV channels 8 and 9 already shows a small decrease of RMSE versus the observations on eight months in 2003, if the slant raypath is considered. With this and on the basis of

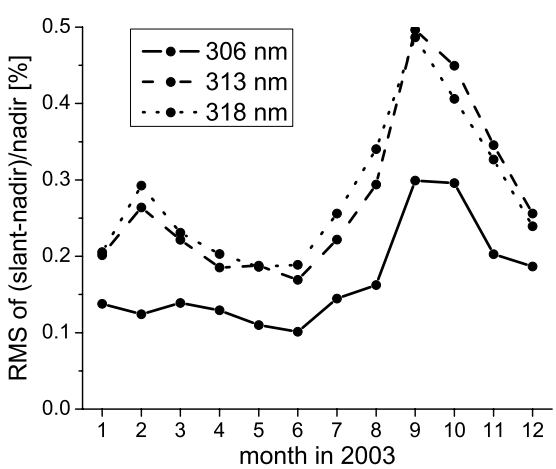

Figure 10. Variation of radiance differences over the year 2003. For each month, days 25–27 were sampled.

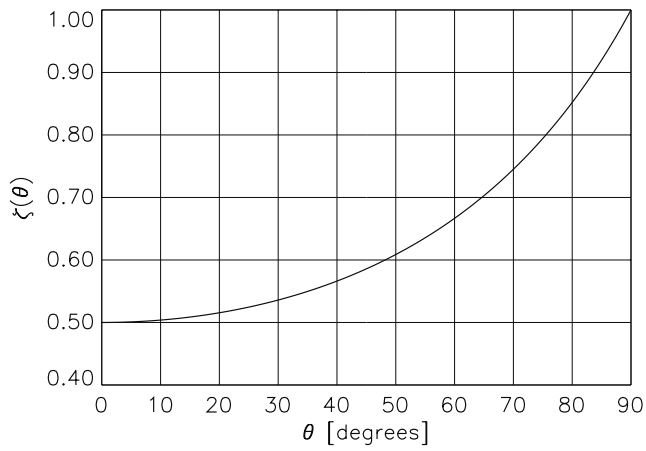

Figure 11. Variation of the mapping factor ζ with angle of incidence θ of the incoming ray. This factor estimates the fraction of slant-nadir radiance difference "seen" by forward modeling.

the results obtained thus far, it is hoped that the additional processor cycles needed to calculate a first-order slant path correction turn out to be a worthwhile investment, compared to the computational effort for performing the analysis.

[27] **Acknowledgments.** The authors wish to thank Ivanka Stajner and Steven Pawson for their extensive help with the GEOS-4 ozone assimilation system. Pawan K. Bhartia provided many valuable insights into the SBUV sensor system. Funding for this research was provided by NASA through a grant from the National Research Council.

References

Bhartia, P. K., R. D. McPeters, C. L. Mateer, L. E. Flynn, and C. Wellemeyer (1996), Algorithm for the estimation of vertical ozone profiles from the backscattered ultraviolet (BUV) technique, *J. Geophys. Res.*, *101*(D13), 18,793–18,806.

Bovensmann, H., J. P. Burrows, M. Buchwitz, J. Frerick, S. Noel, V. Rozanov, K. V. Chance, and A. H. P. Goede (1999), SCIAMACHY—Mission objectives and measurement modes, *J. Atmos. Sci.*, *56*, 125–150.

DeLand, M. T., R. P. Cebula, and E. Hilsenrath (2004), Observations of solar spectral irradiance change during cycle 22 from NOAA-9 Solar Backscattered Ultraviolet Model 2 (SBUV/2), *J. Geophys. Res.*, *109*, D06304, doi:10.1029/2003JD004074.

Dittman, M. G., et al. (2002), Limb broad-band imaging spectrometer for the NPOESS Ozone Mapping and Profiler Suite (OMPS), *Proc. SPIE Int. Soc. Opt. Eng.*, *4814*, 120–130.

Fioletov, V. E., J. B. Kerr, E. W. Hare, G. J. Labow, and R. D. McPeters (1999), An assessment of the world ground-based total ozone network performance from the comparison with satellite data, *J. Geophys. Res.*, *104*(D1), 1737–1747.

Hudson, R. D., A. D. Frolov, M. F. Andrade, and M. B. Follette (2003), The total ozone field separated into meteorological regimes. Part I: Defining the regimes, *J. Atmos. Sci.*, *60*(14), 1669–1677.

Joiner, J., and P. Poli (2005), Note on the effect of horizontal gradients for nadir-viewing microwave and infrared sounders, *Q. J. R. Meteorol. Soc.*, *131*(608), 1783–1792.

Labow, G. J., R. D. McPeters, and P. K. Bhartia (2004), A comparison of TOMS, SBUV, and SBUV/2 version 8 total column ozone data with data from groundstations, paper presented at XX Quadrennial Ozone Symposium, Int. Ozone Comm., Kos, Greece.

Lambert, J.-C., M. V. Roozendael, J. Granville, P. Gérard, P. C. Simon, H. Claude, and J. Staehelin (1998), Comparison of the GOME ozone and NO_2 total amounts at mid-latitude with ground-based zenith-sky measurements, paper presented at XVIII Quadrennial Ozone Symposium, Int. Ozone Comm., L'Aquila, Italy.

Levelt, P. F., G. H. J. van den Oord, M. R. Dobber, A. Mälkki, H. Visser, J. de Vries, P. Stammes, J. Lundell, and H. Saari (2006), The Ozone Monitoring Instrument, *IEEE Trans. Geosci. Rem. Sens.*, *44*(5), 1093–1101, doi:10.1109/TGRS.2006.872333.

Lin, S. J. (2004), A "vertically Lagrangian" finite-volume dynamical core for global models, *Mon. Weather Rev.*, *132*(10), 2293–2307.

Müller, M. D., P. K. Bhartia, and I. Stajner (2004), Assimilation of SBUV version 8 radiances into the GEOS Ozone DAS, paper presented at XX Quadrennial Ozone Symposium, Int. Ozone Comm., Kos, Greece.

Poli, P. (2004), Effects of horizontal gradients on GPS radio occultation observation operators. II: A Fast Atmospheric Refractivity Gradient Operator (FARGO), *Q. J. R. Meteorol. Soc.*, *130*(603), 2807–2825.

Poli, P., and J. Joiner (2004), Effects of horizontal gradients on GPS radio occultation observation operators. I: Ray tracing, *Q. J. R. Meteorol. Soc.*, *130*(603), 2787–2805.

Riishøjgaard, L. P., I. Stajner, and G.-P. Lou (2000), The GEOS ozone data assimilation system, *Adv. Space Res.*, *25*, 1063–1072.

Stajner, I., L. P. Riiøshjgaard, and R. B. Rood (2001), The GEOS ozone data assimilation system: Specification of error statistics, *Q. J. R. Meteorol. Soc.*, *127*(573), 1069–1094.

Stajner, I., N. Winslow, R. B. Rood, and S. Pawson (2004), Monitoring of observation errors in the assimilation of satellite ozone data, *J. Geophys. Res.*, *109*, D06309, doi:10.1029/2003JD004118.

Wargan, K., I. Stajner, S. Pawson, R. B. Rood, and W.-W. Tan (2005), Assimilation of ozone data from the Michelson Interferometer for Passive Atmospheric Sounding, *Q. J. R. Meteorol. Soc.*, *131*, 2713–2734.

Worden, J. R., K. W. Bowman, and D. B. Jones (2004), Two-dimensional characterization of atmospheric profile retrievals from limb sounding observations, *J. Quant. Spectrosc. Radiat. Transfer*, *86*, 45–71.

M. Felder, Leibniz Computing Centre, Boltzmannstraße 1, D-85748 Garching, Germany. (felder@lrz.de)

J. Joiner, Laboratory for Atmospheres, NASA Goddard Space Flight Center, Greenbelt Road, Greenbelt, MD 20771, USA. (joanna.joiner@nasa.gov)

P. Poli, Centre National de Recherches Météorologiques, Météo-France, 42 avenue Gustave-Coriolis, F-31057 Toulouse Cedex 01, France. (paul.poli@meteo.fr)